

# Reconstructing the Surface of Gold Nanoclusters by Cadmium **Doping**

Qi Li,<sup>†</sup> Kelly J. Lambright,<sup>‡</sup> Michael G. Taylor, <sup>||</sup> Kristin Kirschbaum, <sup>‡</sup> Tian-Yi Luo, <sup>§</sup> Jianbo Zhao, <sup>†</sup> Giannis Mpourmpakis, Soumitra Mokashi-Punekar, Nathaniel L. Rosi, and Rongchao Jin\*

Supporting Information

**ABSTRACT:** Atomically precise metal nanoclusters with tailored surface structures are important for both fundamental studies and practical applications. The development of new methods for tailoring the surface structure in a controllable manner has long been sought. In this work, we report surface reconstruction induced by cadmium doping into the  $[Au_{23}(SR)_{16}]^-$  (R = cyclohexyl) nanocluster, in which two neighboring surface Au atomic sites "coalesce" into one Cd atomic site and, accordingly, a new bimetal nanocluster, [Au<sub>19</sub>Cd<sub>2</sub>(SR)<sub>16</sub>]<sup>-</sup>, is produced. Interestingly, a Cd(S-Au-S)<sub>3</sub> "paw-like" surface motif is observed for the first time in nanocluster structures. In such a motif, the Cd atom acts as a junction which connects three monomeric -S-Au-S- motifs. Density functional theory calculations are performed to understand the two unique Cd locations. Furthermore, we demonstrate different doping modes when the [Au<sub>23</sub>(SR)<sub>16</sub>] nanocluster is doped with different metals (Cu, Ag), including (i) simple substitution and (ii) total structure transformation, as opposed to surface reconstruction for Cd doping. This work greatly expands doping chemistry for tailoring the structures of nanoclusters and is expected to open new avenues for designing nanoclusters with novel surface structures using different dopants.

oping, as a process of intentional insertion of heteroatoms into a material, is a ubiquitous methodology for manipulating the properties of nanomaterials. After many years of intense research, scientists have developed excellent skills for the synthesis of doped nanoparticles and, accordingly, have achieved a deeper understanding of the dopants' influences on the nanoparticle properties. 1-3 However, some issues of fundamental importance in the doping of nanoparticles are still not solved yet; for example, what are the exact positions and numbers of dopants in a doped nanoparticle? It is generally presumed that doping involves the addition of heteroatoms into a nanoparticle either substitutionally (i.e., replacing the original atoms) or interstitially (i.e., filling vacant sites).<sup>4a</sup> Moreover, because of the lack of an atomic length-scale structure, 4b it was not possible to conclude explicitly whether doping would alter the original structure of the nanoparticle and, if so, to what

extent. The surface structure of nanoparticles is especially important for catalysis and luminescence as well as charge transport properties, 5,6 but the surface structure is extremely difficult to map out with atomic precision by conventional characterization techniques, such as electron microscopy.<sup>4</sup>

Fortunately, recent research advances on atomically precise ultrasmall metal nanoparticles (often called nanoclusters, size = 1–3 nm) can help answer the above-mentioned questions. 5–7 In the past years, major advances have been achieved in the synthesis of gold, silver, and alloy nanoclusters with definite formulas, and, more importantly, their atomic structures have been solved by single-crystal X-ray analysis.<sup>8,9</sup> The successes in total structure (both metal core and surface) determination with atomic precision constitute a major step toward fundamental understanding of those major unsolved issues of nanoparticle doping, especially the surface structure and precise information on dopants 10-12 which cannot be mapped out by electron microscopy.

Research into the doping chemistry of nanoclusters has revealed a predominant mode—i.e., substitution, which is a simple replacement of original metal atoms by dopant atoms. 11 The majority of the research has focused on Ag, Cu, and Au dopants, while much less work has been done on doping nanoclusters with group IIB metals (Zn, Cd, Hg); <sup>12</sup> in particular, it remains completely unknown how these group IIB dopants would affect the structure and properties of non-icosahedral Au or Ag nanoclusters.

Herein, we present the first case of doping-induced surface reconstruction of a Au nanocluster. Specifically, it is discovered by single-crystal X-ray analysis that Cd doping of the  $[Au_{23}(SR)_{16}]^-$  nanocluster leads to a "coalescence" of two nearby surface Au atomic sites into one Cd site and thus creates a new bimetal nanocluster, [Au<sub>19</sub>Cd<sub>2</sub>(SR)<sub>16</sub>]<sup>-</sup>, with a novel "pawlike" Cd(S-Au-S)<sub>3</sub> surface motif. Density functional theory (DFT) calculations are performed to understand the unique dopant locations in the [Au<sub>19</sub>Cd<sub>2</sub>(SR)<sub>16</sub>] nanocluster. On the other hand, doping the [Au<sub>23</sub>(SR)<sub>16</sub>]<sup>-</sup> nanocluster with Cu only results in substitution of the surface Au atoms in  $[Au_{23}(SR)_{16}]^{-}$ . This work demonstrates that doping can indeed be explored as a useful strategy for tailoring the atomic structure of nanoclusters

Received: October 28, 2017 Published: November 28, 2017

<sup>&</sup>lt;sup>†</sup>Department of Chemistry, Carnegie Mellon University, Pittsburgh, Pennsylvania 15213, United States

<sup>&</sup>lt;sup>‡</sup>College of Natural Sciences and Mathematics, University of Toledo, Toledo, Ohio 43606, United States

Department of Chemical Engineering, University of Pittsburgh, Pittsburgh, Pennsylvania 15261, United States

<sup>§</sup>Department of Chemistry, University of Pittsburgh, Pittsburgh, Pennsylvania 15260, United States

and reveals that both the type and concentration of dopant are critical in determining the final structure of the doped products.

The  $[Au_{19}Cd_2(SR)_{16}]^-$  nanocluster was obtained via doping  $[Au_{23}(SR)_{16}]^-$  with  $Cd^{II}(SR)_2$  (R = cyclohexyl, see Supporting Information (SI) for details). The total structure of  $[Au_{19}Cd_2(SR)_{16}]^-$  (counterion:  ${}^+N(C_8H_{17})_4$ ,  $TOA^+$  for short) is shown in Figure 1A. A comparison of the  $[Au_{23}(SR)_{16}]^-$  and

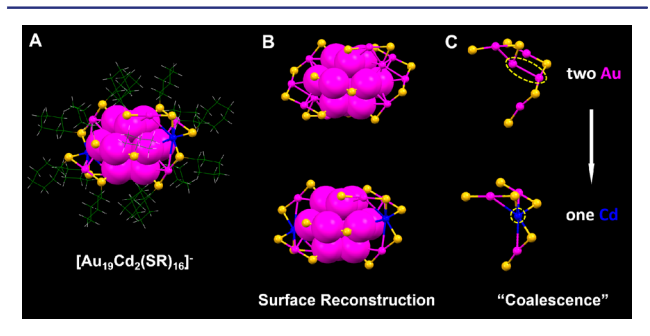
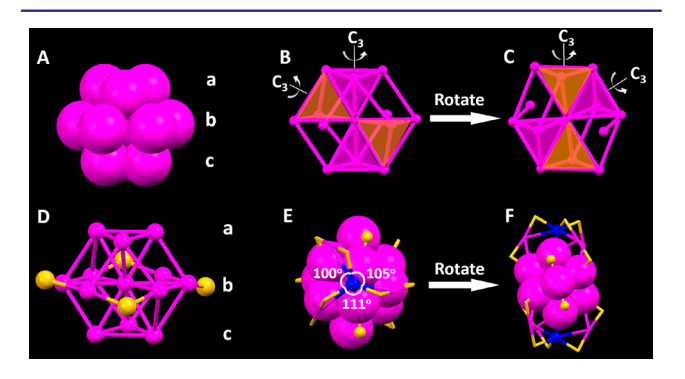


Figure 1. (A) Total structure of [Au<sub>19</sub>Cd<sub>2</sub>(SR)<sub>16</sub>]<sup>-</sup>. (B) Comparison of  $[Au_{23}(SR)_{16}]^-$  (upper, ref 8a) and  $[Au_{19}Cd_2(SR)_{16}]^-$  (lower). (C) Comparison of the surface motif of  $[Au_{23}(SR)_{16}]^-$  (upper) and [Au<sub>19</sub>Cd<sub>2</sub>(SR)<sub>16</sub>]<sup>-</sup> (lower), and "coalescence" of two nearby surface Au atom sites to one Cd atom site. Color code: magenta = Au, blue = Cd, yellow = S, green = C, white = H. The Au atoms in the  $Au_{13}$  core are displayed in space-filling mode; Cd, S, and other Au atoms are in balland-stick mode. The C and H atoms are shown in wireframe in (A) and omitted for clarity in (B). The counterion (TOA+) is omitted.

 $[Au_{19}Cd_2(SR)_{16}]^-$  structures (Figure 1B) shows the same  $Au_{13}$ cuboctahedral core, but different surface structures. It can be seen that  $[Au_{19}Cd_2(SR)_{16}]^-$  results from "surface reconstruction" of [Au<sub>23</sub>(SR)<sub>16</sub>] upon Cd doping. This surface reconstruction occurs via "coalescence" of two neighboring surface Au atom sites into one Cd site (Figure 1C); thus, the original staple motifs (including one monomeric motif -S-Au-S- and one trimeric -S-Au-S-Au-S-Au-S- motif) become a "paw-like" Cd(S-Au-S)<sub>3</sub> motif, in which the Cd atom joins the three -S-Au-S- monomers.

Figure 2 shows the anatomy of the [Au<sub>19</sub>Cd<sub>2</sub>(SR)<sub>16</sub>] structure. The Au<sub>13</sub> cuboctahedral core (Figure 2A) comprises three layers (i.e., Au<sub>3</sub>-Au<sub>7</sub>-Au<sub>3</sub>) in an a-b-c manner, 8a hence, a face-centered-cubic (FCC) structure. Four vertex-sharing Au<sub>4</sub> tetrahedra can be identified along the two quasi C<sub>3</sub> axes, forming



**Figure 2.** Anatomy of the X-ray crystal structure of  $[Au_{19}Cd_2(SR)_{16}]^-$ : (A) Au<sub>13</sub> cuboctahedron core in space-filling mode; (B,C) four tetrahedral Au<sub>4</sub> units in the Au<sub>13</sub> core; (D) the Au<sub>13</sub> cuboctahedral core protected by four bridging SR motifs; (E,F) different views of the tripodal  $Cd(S-Au-S)_3$  surface "paws" that protect the  $Au_{13}$  cuboctahedral core. Color code: magenta = Au, blue = Cd, yellow = S. All C and H atoms are omitted for clarity.

two "dumbbells" (Figure 2B,C). These tetrahedra exhibit much shorter Au-Au bond lengths (average 2.73 Å in one dumbbell and 2.85 Å in the other) within each tetrahedron in comparison to the bond lengths outside the tetrahedral unit. The Au<sub>13</sub> cuboctahedron is protected by four bridging -S(R)- ligands along the middle b layer (Figure 2D) and two Cd(S-Au-S)<sub>3</sub> surface "paws" (Figure 2E,F). The bond angles of the three S-Cd-S in the Cd(S-Au-S)<sub>3</sub> motifs are ~105°, ~111°, and ~100°. This configuration is reminiscent of the zincblende structure of CdS crystal in which every Cd connects four S atoms, <sup>1,6a</sup> constituting a tetrahedron with S-Cd-S bond angle of ~109°. Each [Au<sub>19</sub>Cd<sub>2</sub>(SR)<sub>16</sub>] cluster is associated with one counterion  $(TOA^+)$ , indicating a -1 charge for the cluster.

The absorption spectrum of  $[Au_{19}Cd_2(SR)_{16}]^-$  is displayed in Figure S1A. A distinct peak at ~586 nm can be observed, and the ~10 nm red-shift of the peak compared with the [Au<sub>23</sub>(SR)<sub>16</sub>]<sup>-8a</sup> indicates that the atomic orbital of Cd does contribute to the HOMO- LUMO transition. The anionic nature of the cluster is confirmed by electrospray ionization mass spectrometry (ESI-MS, negative mode), which shows a single peak at  $5811 \, m/z$  (Figure S1B). The unity spacing of the isotope peaks indicates the -1 charge of the cluster. The isotope pattern is fully consistent with the calculated one (Figure S1B inset). It is worth mentioning that the nominal count of metal core free valence electrons (Au 6s<sup>1</sup> and Cd 5s<sup>2</sup>) is 8e in view of the thiolate ligand being monovalent; thus,  $[Au_{19}Cd_2(SR)_{16}]^-$  is isoelectronic with the parent cluster  $[Au_{23}(SR)_{16}]^{-.8a}$  The charge state of Cd was further evaluated by X-ray photoelectron spectroscopy (Figure S2), indicating its contribution to the valence electrons of the cluster.

To probe the catalytic effect of the different surface structures of  $[Au_{19}Cd_2(SR)_{16}]^-$  and  $[Au_{23}(SR)_{16}]^-$ , these nanoclusters were evaluated in two catalytic reactions (see SI for details). Interestingly, [Au<sub>19</sub>Cd<sub>2</sub>(SR)<sub>16</sub>] shows a distinctly enhanced catalytic activity from 48% (undoped) to 63% (doped) in the hydrogenation of nitrobenzaldehyde in water (Table S1), but a decreased catalytic activity for the A<sup>3</sup> coupling reaction (from 50% to 14%, Table S2). These results demonstrate that the Cddoping-induced surface reconstruction has a strong influence on the catalytic properties of the nanocluster, with the hydrogenation and A<sup>3</sup> coupling reactions exhibiting opposite effects. In addition, Hg and Zn doping were also tried, but decomposition of  $[Au_{23}(SR)_{16}]^-$  occurred. More careful tuning of the precursors and doping conditions is still needed to achieve such doping.

To develop better understanding on the unique dopant locations of the [Au<sub>19</sub>Cd<sub>2</sub>(SR)<sub>16</sub>] nanocluster, we performed DFT calculations. To simplify the calculations, cyclohexanethiolate groups were substituted by methyl groups. Figure 3 shows the calculated structural and electronic characteristics as well as the energy preference of various [Au<sub>19</sub>Cd<sub>2</sub>(SR)<sub>16</sub>]<sup>-</sup> isomers, where the first Cd atom is placed on the experimentally determined position and the second Cd is randomly placed on one of the remaining metal positions of the cluster. First, we note that over geometry relaxation the [Au<sub>19</sub>Cd<sub>2</sub>(SR)<sub>16</sub>] nanocluster with the Cd dopants at the experimental positions (labeled (9) in Figure 3A) is a stable cluster with little geometric displacement ( $\delta$ ). However, when this  $[Au_{19}Cd_2(SR)_{16}]^-$  cluster has just one of the Cd positions shifted, in most cases the cluster becomes unstable under relaxation, displaying significant geometric displacement ( $\delta$ ), cases (1)–(8), see Figure 3B. Furthermore, the two additional doping positions that do not displace, (10) and (11), are of higher Gibbs free energy (approximately +65 kJ/ mol, Figure 3B) than the experimentally determined doping

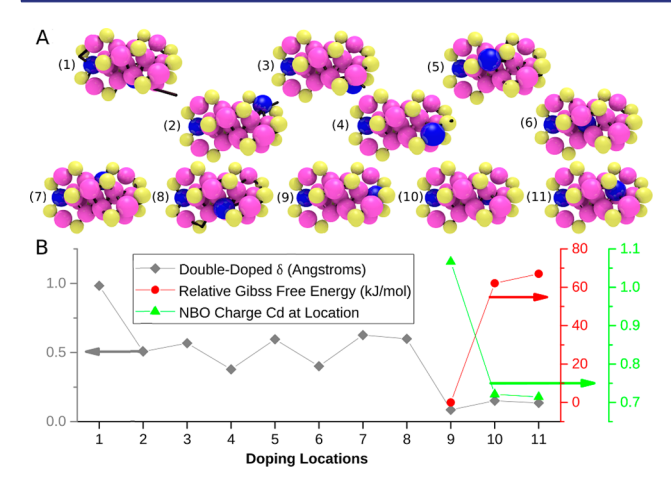


Figure 3. DFT results for [Au<sub>19</sub>Cd<sub>2</sub>(SR)<sub>16</sub>] with Cd dopants shifted to different locations, where doping location (9) represents the experimentally observed structure. (A) Experimental nanocluster geometries before (ball-and-stick) and after (black sticks) geometry relaxation. In the ball-and-stick representations, magenta = Au, blue = Cd, and yellow = S. All C and H atoms are omitted for clarity. (B) Doping locations compared to geometric rearrangement, Gibbs free energy, and Natural Bond Orbital (NBO) charge (see SI, DFT methods discussion, for more information on NBO). For clusters with  $\delta > 0.2$  Å, the free energies and NBO charges have been omitted due to their geometric reconstruction.

position (9), highlighting the unique preference of Cd doping positions in this nanocluster. For comparison, the energetic difference between Ag doping positions within the [Au<sub>23</sub>(SR)<sub>16</sub>] - cluster previously reported<sup>10a</sup> were closer to  $+10 \,\mathrm{kJ/mol}$ . For the three doping positions ((9), (10), and (11)) that did not displace (in Figure 3), the charge state of the dopants trends exactly with the energetic preference of the dopants in these positions, as observed in our previous study of Ag doping into the Au<sub>24</sub>(SR)<sub>20</sub> nanocluster. <sup>10c</sup> Additionally, when only either one or both Cd are replaced with Au in the [Au<sub>10</sub>Cd<sub>2</sub>(SR)<sub>16</sub>] framework, the cluster deforms, regardless of the dopant position (see Figure S3). All the DFT results (energies, displacement, and charges) for both the single- and double-doped clusters are presented in Table S3. Taken together, the DFT results suggest that the presence of this unique "pawlike" surface motif, formed in the presence of Cd, makes backreplacement of Cd with Au unfavorable.

Interestingly, reducing the amount of Cd<sup>II</sup>(SR)<sub>2</sub> in the synthesis (see SI for details) leads to the formation of 23metal-atom alloy  $[Au_{23-x}Cd_x(SR)_{16}]^-$  ( $x\approx 2.3$ ), instead of the 21-metal-atom bimetallic  $[Au_{19}Cd_2(SR)_{16}]^-$  nanocluster. The Xray structure of  $[Au_{23-x}Cd_x(SR)_{16}]^-$  is solved (Figure S4A), which shows the same structure of  $[Au_{23}(SR)_{16}]^-$  except the substitution of two surface Au atoms by Cd atoms with partial occupancy. Specifically, the atomic percentages of Cd in positions 1 and 2 (Figure S4A) are 0.55 and 0.60, respectively (Table S4), and the X-ray composition is determined to be [Au<sub>20.7</sub>Cd<sub>2.3</sub>(SR)<sub>16</sub>]<sup>-</sup>. A counterion (TOA<sup>+</sup>) was also identified along with the cluster; thus, the -1 charge was retained in the Cd-doped 23-atom cluster. The absorption spectrum of the  $[Au_{23-x}Cd_x(SR)_{16}]^-$  is shown in Figure S4B, with a peak at ~579 nm, which is slightly red-shifted compared with that of  $[Au_{23}(SR)_{16}]^-$  (~575 nm).

In addition, Cu-doped  $[Au_{23-x}Cu_x(SR)_{16}]^-$  was synthesized, and its X-ray structure was obtained (Figure S5). The Cu dopants were found exclusively on the surface staples (including the monomers and trimers). The occupancy of Cu dopant at the four surface positions is 47.2%, 11.5%, 8.2%, and 15%, respectively (Table S5). The X-ray crystallographically averaged composition is  $[Au_{21,34}Cu_{1.66}(SR)_{16}]^{-}$ . A counterion  $(TOA^{+})$ was also found, with 1:1 ratio of TOA+/cluster, indicating that the -1 charge is also retained in the Cu-doped  $[Au_{23-x}Cu_x(SR)_{16}]^-$  cluster. Being different from the Cd doping case, Cu doping of  $[Au_{23}(SR)_{16}]^-$  only leads to the substitution of the surface-motif Au atoms without altering any structure. Of note, we found that dramatically increasing the dopant Cu<sup>II</sup>(SR)<sub>2</sub> precursor concentration in the synthesis would induce the decomposition of nanoclusters. The optical absorption spectrum of [Au<sub>23-r</sub>Cu<sub>r</sub>(SR)<sub>16</sub>] is shown in Figure S5B, which shows a peak at ~570 nm. The composition of  $[Au_{23-r}Cu_r(SR)_{16}]^-$  was further analyzed by ESI-MS (Figure S5B, inset), with up to three copper atoms being doped into  $[Au_{23}(SR)_{16}]^{-}$ .

Figure 4 summarizes the structural information on [Au<sub>23</sub>(SR)<sub>16</sub>]<sup>-</sup> through doping with different metals (Cu, Cd,

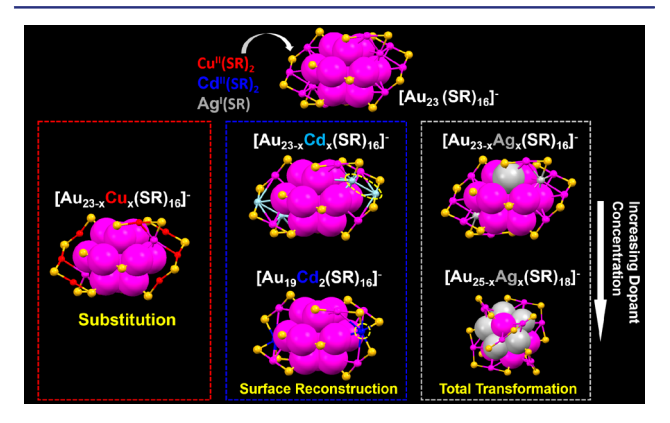


**Figure 4.** Schematic diagram of the structure evolution of  $[Au_{23}(SR)_{16}]^{-1}$ by doping with different metal-thiolate complexes. Color code: magenta = Au; gray = partial occupancy of Ag/Au, blue = Cd, light blue = partial occupancy of Cd/Au, red = partial occupancy of Cu/Au, yellow = S. All C and H atoms are omitted for clarity.

and Ag10a), which reveals three different doping modes, including (i) simple substitution, (ii) surface reconstruction, and (iii) total structure transformation. Among the dopants, Cu doping (left panel, Figure 4) results in only substitution of surface Au atoms without causing any structural change, which is the simplest case. On the other hand, for Cd doping of  $[Au_{23}(SR)_{16}]^-$  (middle panel, Figure 4), two specific surface Au atoms are first substituted by Cd with partial occupancy under slight doping. By increasing the amount of dopant Cd, the two specific Au sites "coalesce" into one Cd site (with no partial occupancy), which induces a reconstruction of the surface motif and results in a new cluster, [Au<sub>19</sub>Cd<sub>2</sub>(SR)<sub>16</sub>]<sup>-</sup>. In addition, our previous work reported  $[Au_{25} Ag_x(SR)_{16}]^-$  synthesized from  $[Au_{23}(SR)_{16}]^-$  through heavy doping of Ag (right panel, Figure 4), which led to a transformation of the total structure (both core and surface) by increasing the dopant Ag concentration. 10b Meanwhile, it can be summarized from both experimental and theoretical results that the dopant concentration is critical: the original structure of  $[Au_{23}(\bar{SR})_{16}]^-$  is retained under slight doping, but it starts to change under high concentrations of Cd and Ag dopants. All the above results suggest that doping in nanoclusters is not just a simple substitution of original atoms or filling a vacant site; instead, it can be explored as a useful method

to tailor the structure of nanoclusters partially (e.g., Cd doping of  $Au_{23}$ ) or totally (e.g., Ag doping of  $Au_{23}$ ).

In summary, we have demonstrated a new doping mode in Au nanoclusters, that is, "coalescence" of two Au atomic sites into one Cd atom site, which is in striking contrast with the previously reported substitutional doping. This new doping mode of Cd leads to a surface reconstruction of the parent Au nanocluster and thus creates a new bimetal nanocluster, [Au<sub>19</sub>Cd<sub>2</sub>(SR)<sub>16</sub>]<sup>-</sup>, with novel Cd(S-Au-S)<sub>3</sub> "paw-like" motifs. Overall, this work demonstrates the intriguing chemistry of doping for tailoring the atomic structures of nanoclusters and reveals that both the type and concentration of dopants are critical in controlling the final structures of the doped products. This work greatly expands the horizons of doping chemistry and its effects on the structure of nanoclusters.

#### ASSOCIATED CONTENT

# Supporting Information

The Supporting Information is available free of charge on the ACS Publications website at DOI: 10.1021/jacs.7b11491.

Experimental and DFT details, syntheses of nanoclusters, X-ray analyses, Figures S1-S5, and Tables S1-S10 (PDF) X-ray crystal data for  $[Au_{19}Cd_2(SR)_{16}]^-[TOA]^+$  (CIF) X-ray crystal data for  $[Au_{23-x}Cd_x(SR)_{16}]^-[TOA]^+$  (CIF) X-ray crystal data for  $[Au_{23-x}Cu_x(SR)_{16}]^-[TOA]^+$  (x = 1.66) (CIF)

## AUTHOR INFORMATION

### **Corresponding Author**

\*rongchao@andrew.cmu.edu

ORCID

Tian-Yi Luo: 0000-0002-9973-9328

Giannis Mpourmpakis: 0000-0002-3063-0607 Nathaniel L. Rosi: 0000-0001-8025-8906 Rongchao Jin: 0000-0002-2525-8345

**Notes** 

The authors declare no competing financial interest.

## **ACKNOWLEDGMENTS**

R.J. acknowledges financial support from the Air Force Office of Scientific Research under Award No. FA9550-15-1-9999 (FA9550-15-1-0154). G.M. acknowledges support by the National Science Foundation (NSF, CBET-CAREER program) under Grant No. 1652694, and M.G.T. acknowledges support by the NSF Graduate Research Fellowship under Grant No. 1247842. Computational support was provided by the University of Pittsburgh Center for Research Computing and the Extreme Science and Engineering Discovery Environment supported by the NSF (ACI-1548562).

## REFERENCES

- (1) (a) Yang, Y.; Chen, O.; Angerhofer, A.; Cao, Y. C. J. Am. Chem. Soc. 2008, 130, 15649. (b) Nelson, H. D.; Hinterding, S. O. M.; Fainblat, R.; Creutz, S. E.; Li, X.; Gamelin, D. R. J. Am. Chem. Soc. 2017, 139, 6411. (c) Yang, J.; Muckel, F.; Baek, W.; Fainblat, R.; Chang, H.; Bacher, G.; Hyeon, T. J. Am. Chem. Soc. 2017, 139, 6761.
- (2) Huang, X.; Zhao, Z.; Cao, L.; Chen, Y.; Zhu, E.; Lin, Z.; Li, M.; Yan, A.; Zettl, A.; Wang, Y. M.; Duan, X.; Mueller, T.; Huang, Y. Science 2015,
- (3) Norris, D. J.; Efros, A. L.; Erwin, S. C. Science 2008, 319, 1776.
- (4) (a) Kroupa, D. M.; Hughes, B. K.; Miller, E. M.; Moore, D. T.; Anderson, N. C.; Chernomordik, B. D.; Nozik, A. J.; Beard, M. C. J. Am.

- Chem. Soc. 2017, 139, 10382. (b) Owen, J. S.; Brus, L. E. J. Am. Chem. Soc. 2017, 139, 10939.
- (5) Liu, P.; Qin, R.; Fu, G.; Zheng, N. J. Am. Chem. Soc. 2017, 139,
- (6) (a) Lin, J.; Zhang, Q.; Wang, L.; Liu, X.; Yan, W.; Wu, T.; Bu, X.; Feng, P. J. Am. Chem. Soc. 2014, 136, 4769. (b) Femoni, C.; Iapalucci, M. C.; Longoni, G.; Zacchini, S.; Zarra, S. J. Am. Chem. Soc. 2011, 133, 2406. (7) (a) Jin, R.; Zeng, C.; Zhou, M.; Chen, Y. Chem. Rev. 2016, 116, 10346. (b) Kurashige, W.; Niihori, Y.; Sharma, S.; Negishi, Y. Coord. Chem. Rev. 2016, 320-321, 238. (c) Chakraborty, I.; Pradeep, T. Chem. Rev. 2017, 117, 8208. (d) Fernando, A.; Weerawardene, K. L. D. M.; Karimova, N. V.; Aikens, C. M. Chem. Rev. 2015, 115, 6112. (e) Yau, S. H.; Varnavski, O.; Goodson, T. Acc. Chem. Res. 2013, 46, 1506. (f) Xu, W. W.; Zhu, B.; Zeng, X. C.; Gao, Y. Nat. Commun. 2016, 7, 13574.
- (g) Taylor, M. G.; Mpourmpakis, G. Nat. Commun. 2017, 8, 15988. (h) Yamazoe, S.; Takano, S.; Kurashige, W.; Yokoyama, T.; Nitta, K.; Negishi, Y.; Tsukuda, T. Nat. Commun. 2016, 7, 10414.
- (8) (a) Das, A.; Li, T.; Nobusada, K.; Zeng, C.; Rosi, N. L.; Jin, R. J. Am. Chem. Soc. 2013, 135, 18264. (b) Wan, X.-K.; Tang, Q.; Yuan, S.-F.; Jiang, D.-e.; Wang, Q.-M. J. Am. Chem. Soc. 2015, 137, 652. (c) Desireddy, A.; Conn, B. E.; Guo, J.; Yoon, B.; Barnett, R. N.; Monahan, B. M.; Kirschbaum, K.; Griffith, W. P.; Whetten, R. L.; Landman, U.; Bigioni, T. P. Nature 2013, 501, 399. (d) AbdulHalim, L. G.; Bootharaju, M. S.; Tang, Q.; Del Gobbo, S.; AbdulHalim, R. G.; Eddaoudi, M.; Jiang, D.-e.; Bakr, O. M. J. Am. Chem. Soc. 2015, 137, 11970. (e) Crasto, D.; Barcaro, G.; Stener, M.; Sementa, L.; Fortunelli, A.; Dass, A. J. Am. Chem. Soc. 2014, 136, 14933. (f) Dhayal, R. S.; Liao, J. H.; Liu, Y. C.; Chiang, M. H.; Kahlal, S.; Saillard, J. Y.; Liu, C. Angew. Chem., Int. Ed. 2015, 54, 3702.
- (9) (a) Ren, L.; Yuan, P.; Su, H.; Malola, S.; Lin, S.; Tang, Z.; Teo, B. K.; Häkkinen, H.; Zheng, L.; Zheng, N. J. Am. Chem. Soc. 2017, 139, 13288. (b) Yang, H.; Yan, J.; Wang, Y.; Su, H.; Gell, L.; Zhao, X.; Xu, C.; Teo, B. K.; Häkkinen, H.; Zheng, N. J. Am. Chem. Soc. 2017, 139, 31. (c) Yang, H.; Wang, Y.; Chen, X.; Zhao, X.; Gu, L.; Huang, H.; Yan, J.; Xu, C.; Li, G.; Wu, J.; Edwards, A. J.; Dittrich, B.; Tang, Z. C.; Wang, D. D.; Lehtovaara, L.; Häkkinen, H.; Zheng, N. Nat. Commun. 2016, 7, 12809. (d) Zeng, J.-L.; Guan, Z.-J.; Du, Y.; Nan, Z.-A.; Lin, Y.-M.; Wang, Q.-M. J. Am. Chem. Soc. 2016, 138, 7848. (e) Wan, X.-K.; Cheng, X.-L.; Tang, Q.; Han, Y.-Z.; Hu, G.; Jiang, D.-e.; Wang, Q.-M. J. Am. Chem. Soc. 2017, 139, 9451. (f) Alhilaly, M. J.; Bootharaju, M. S.; Joshi, C. P.; Besong, T. M.; Emwas, A.-H.; Juarez-Mosqueda, R.; Kaappa, S.; Malola, S.; Adil, K.; Shkurenko, A.; Häkkinen, H.; Eddaoudi, M.; Bakr, O. M. J. Am. Chem. Soc. 2016, 138, 14727. (g) Bootharaju, M. S.; Kozlov, S. M.; Cao, Z.; Harb, M.; Maity, N.; Shkurenko, A.; Parida, M. R.; Hedhili, M. N.; Eddaoudi, M.; Mohammed, O. F.; Bakr, O. M.; Cavallo, L.; Basset, J.-M. J. Am. Chem. Soc. 2017, 139, 1053. (h) Qu, M.; Li, H.; Xie, L.-H.; Yan, S.-T.; Li, J.-R.; Wang, J.-H.; Wei, C.-Y.; Wu, Y.-W.; Zhang, X.-M. J. Am. Chem. Soc. 2017, 139, 12346. (i) Kenzler, S.; Schrenk, C.; Schnepf, A. Angew. Chem., Int. Ed. 2017, 56, 393. (j) Kwak, K.; Tang, Q.; Kim, M.; Jiang, D.-e.; Lee, D. J. Am. Chem. Soc. 2015, 137, 10833. (k) Barrabés, N.; Zhang, B.; Bürgi, T. J. Am. Chem. Soc. 2014, 136, 14361.
- (10) (a) Li, Q.; Luo, T.-Y.; Taylor, M. G.; Wang, S.; Zhu, X.; Song, Y.; Mpourmpakis, G.; Rosi, N. L.; Jin, R. Sci. Adv. 2017, 3, e1603193. (b) Li, Q.; Wang, S.; Kirschbaum, K.; Lambright, K. J.; Das, A.; Jin, R. Chem. Commun. 2016, 52, 5194. (c) Li, Q.; Taylor, M. G.; Kirschbaum, K.; Lambright, K. J.; Zhu, X.; Mpourmpakis, G.; Jin, R. J. Colloid Interface Sci. **2017**, 505, 1202.
- (11) (a) Bootharaju, M. S.; Joshi, C. P.; Parida, M. R.; Mohammed, O. F.; Bakr, O. M. Angew. Chem. 2016, 128, 934. (b) Kumara, C.; Gagnon, K. J.; Dass, A. J. Phys. Chem. Lett. 2015, 6, 1223. (c) Kumara, C.; Aikens, C. M.; Dass, A. J. Phys. Chem. Lett. 2014, 5, 461.
- (12) (a) Yao, C.; Lin, Y.-j.; Yuan, J.; Liao, L.; Zhu, M.; Weng, L.-h.; Yang, J.; Wu, Z. J. Am. Chem. Soc. 2015, 137, 15350. (b) Wang, S.; Song, Y.; Jin, S.; Liu, X.; Zhang, J.; Pei, Y.; Meng, X.; Chen, M.; Li, P.; Zhu, M. J. Am. Chem. Soc. 2015, 137, 4018. (c) Liao, L.; Zhou, S.; Dai, Y.; Liu, L.; Yao, C.; Fu, C.; Yang, J.; Wu, Z. J. Am. Chem. Soc. 2015, 137, 9511.